Effect of the order of Ni and Ce addition in SBA-15 on the activity in dry reforming of methane

Marie-Nour Kaydouh, Nissrine El Hassan, Anne Davidson, Sandra Casale, Pascale Massiani

Effect of the order of Ni and Ce addition in SBA-15 on the activity in dry reforming of methane

Effet de l'ordre d'ajout du Ni et du Ce dans SBA-15 sur l'activité en reformage à sec du methane

Marie-Nour Kaydouh,[1,2] Nissrine El Hassan,[1]* Anne Davidson,[2] Sandra Casale,[2] Pascale Massiani[2,3]*

[1] *Department of Chemical Engineering, Faculty of Engineering, University of Balamand, PO Box 100, Tripoli, Lebanon*

[2] *Sorbonne Universités, UPMC Université Paris 06, Laboratoire de Réactivité de Surface, 4 place Jussieu, 75005 Paris, France*

[3] *CNRS UMR 7197, UPMC, Laboratoire de Réactivité de Surface, 4 place Jussieu, 75005 Paris, France*

Email addresses, phone and fax numbers:

Marie-Nour Kaydouh : marie.kaydouh@std.balamand.edu.lb, Tel : 00961 6 930 250 (5326), Fax : 961 6 930 278

Nissrine El Hassan : nissrine.hassan@balamand.edu.lb, Tel : 00961 6 930 250 (5345), Fax : 961 6 930 278

Anne Davidson : anne.davidson@upmc.fr, Tel : 0033 1 44 27 42 96, Fax : 00 33 1 44 27 60 33

Sandra Casale : sandra.casale@upmc.fr, Tel : 0033 1 44 27 41 35, Fax : 00 33 1 44 27 60 33

Pascale Massiani : pascale.massiani@upmc.fr, Tel : 0033 1 44 27 49 74, Fax : 00 33 1 44 27 60 33

Abstract

Dry reforming of methane has been carried out on SBA-15 catalysts containing 5 wt% Ni and 6 wt% Ce. The effect of the order of Ni and Ce impregnation on the catalytic activity has been studied. Both metals were added using the "two solvents" method that favors metal dispersion inside the pores. Characterizations by XRD (low and high angles), N_2 sorption, SEM and TEM of the materials after metal addition and calcination indicate good preservation of the porosities and high NiO and CeO_2 dispersion inside the porous channels. Reduction was carried out before catalytic tests and followed by TPR measurements. The most active reduced catalyst was the Ni-Ce/SBA-15 sample prepared by impregnating cerium first, then nickel. All catalysts were highly active and selective towards H_2 and CO at atmospheric pressure. Full CH_4 conversion was obtained below $650^{\circ}C$. The higher performances compared to those reported in literature for mesoporous silica with supported Ni and Ce catalysts are discussed.

Keywords: methane dry reforming, mesoporous SBA-15 silica, nickel, cerium, impregnation

Résumé

Le reformage à sec du méthane a été étudié sur des catalyseurs SBA-15 contenant 5% en poids de Ni et 6% en poids de Ce. L'effet de l'ordre d'imprégnation de Ni et Ce sur l'activité catalytique a été étudié. Ces deux métaux ont été ajoutés en utilisant la méthode à "deux solvants" qui favorise la dispersion du métal à l'intérieur des pores. La caractérisation par DRX (petits et grands angles), adsorption de N_2, MEB et MET des matériaux après ajout du métal et calcination montre une bonne préservation de la porosité et une grande dispersion des nanoparticules de NiO et CeO_2 à l'intérieur des pores. La réduction des catalyseurs suivie par RTP a été effectuée avant tests catalytiques. Le catalyseur le plus actif est le Ni-Ce/SBA-15 réduit préparé par imprégnation du cérium tout d'abord, puis du nickel. Les catalyseurs

étaient très actifs et sélectifs en H_2 et CO sous pression atmosphérique, avec une conversion complète de CH_4 atteinte avant 650°C. Les performances supérieures à celle décrites dans la littérature pour des catalyseurs à base de silice mésoporeuse contenant du Ni et du Ce sont discutées.

Mots clés: reformage à sec du méthane, silice mésoporeuse SBA-15, nickel, cérium, imprégnation

1. Introduction

Dry reforming of methane ($CH_4 + CO_2 \rightarrow 2H_2 + 2CO$) is an attractive process that allows the production of recoverable compounds from the utilization of two major greenhouse gases, namely methane and carbon dioxide. This reaction has an important positive environmental impact since behind the widely known deleterious effect of CO_2, methane has a global warming potential roughly 25 times greater than that of carbon dioxide, even with lower amounts in the atmosphere [1]. The second important benefit of the dry reforming reaction is both economic and energetic. Methane is indeed the major component of natural gas that is mainly found in remote areas. Thus, to prevent cost ineffective CH_4 gas transportation, on-site gas-to-liquid transformation via the DRM would be interesting. The dry reforming reaction (DRM) could therefore play a critical role by converting CH_4 and CO_2 into a syngas with hydrogen and carbon monoxide in equimolar ratio that can be directly used in Fischer Tropsch Synthesis for the production of liquid hydrocarbons with high selectivity. However, a drawback of DRM is its endothermic character and the requirement of large amounts of energy.

Recent studies on DRM catalysts have mainly focused on Ni-based systems that are comparably as active as noble metals but more available and less expensive [2,3]. Nevertheless, the high sensitivity of the dispersed Ni active phase to both carbon deposition and to sintering constitutes essential drawbacks that still hinder the use of these catalysts in industrial applications. A suggested solution to inhibit carbon deposition is to promote the catalyst with a metal oxide, especially CeO_2. The latter is characterized by redox properties ($Ce^{4+} \leftrightarrow Ce^{3+}$) that promote oxygen vacancies formation, thus enhancing the mobility of surface oxygen whose presence contributes in lowering carbon deposition on the metallic particles [4-7]. It was also reported that both metal dispersion and metal-support interaction

4

are improved in presence of CeO_2 [5,7]. Moreover, the recent use of organized mesoporous silica [8] and carbon [9,10] supports to disperse the Ni active phase appears promising. Mesoporous SBA-15 materials in particular have distinct properties (high specific surface area, uniform narrow pore size distribution, confinement effect…) known to favor metal dispersion and limit particles sintering, with consequently interesting performances in DRM [5,6].

Few papers, listed in Table 1, have already discussed the effect of the addition of CeO_2 to nickel catalysts on organized mesopourous silica supports. In a Ce-free Ni/SBA-15 catalyst, Wang et al. [5] reported the formation of large Ni particles resulting in heavy coke deposition whereas in presence of cerium high nickel dispersion inside the SBA-15 channels was obtained, the Ce-enriched catalyst was moreover rather stable with minor effect of the formed carbon nanotubes on the main catalytic reaction. Nevertheless, the Ce/Si atomic ratio had to be kept below 0.04 to avoid pore blocking. In another work focused on the promotion of Ni-based SBA-15 catalysts with Ceria-Zirconia mixed oxides (CZ) [6], formation of clustered layers of CZ and NiO phases occurred, which also led to partial or complete blockage of the pores. Consequently, low metal dispersion and very slight enhancement of the catalytic stability were obtained in spite of the presence of ceria. In SBA-16 supported catalysts [7], the Ce addition also improved both nickel dispersion and catalytic stability but comparable coke deposition (mainly of C_β type) was observed with and without Ce. However, migration of Ni particles to the external surface of the support and structural collapse of SBA-16 were inhibited in presence of Ce.

From these previous works, the effect of CeO_2 on mesoporous Ni/oxide catalysts seems to be important in increasing the dispersion of the Ni particle size and stabilizing it during reaction. Nevertheless, in a recent study on preparation of Ni/SBA-15 catalysts for DRM [11], we obtained high and stable nickel dispersions by applying a "two solvent" method of

impregnation [13-15] that allowed full deposition of the metal nanoparticles inside the pores. Moreover, at the medium reaction temperatures applied (500-650°C), the addition of cerium had only a minor effect on both Ni dispersion and catalytic activity. In the continuation of this work, our purpose here is to study in more details the influence of the addition of Ce on the DRM performances of Ni/SBA-15 catalysts prepared by the "two solvents" impregnation method. More precisely, the focal point will be to identify the possible effect of the order of Ni and Ce addition. The dispersion of the active phase after thermal activation as well as the catalytic activity and stability of the catalysts after reduction will be presented.

(Table 1)

2. Experimental part

2.1. Catalysts preparation

The SBA-15 silica support was synthesized according to the method established by Zhao et al. [12]. After filtration, the powders were calcined at $500^{o}C$ (heating rate $2^{o}C.min^{-1}$) for about 9 hours in a muffle furnace (Nabertherm, LE6/11) in order to remove the organic template and the Cl ions. The nickel nitrate ($Ni(NO_3)_2.6H_2O$) or cerium nitrate ($Ce(NO_3)_3.6H_2O$) salts (from Sigma-Aldrich) were then impregnated using the "two solvents" technique, described elsewhere [13-15], that favors the deposition of the metal precursor species inside the pores of the SBA-15 supports. The cerium content was fixed to 6 wt% and that of nickel to 5 wt%. After each impregnation, the sample was calcined in air at 450°C for 5h previous to further treatment. Even if calcination in air has been reported to be detrimental to the dispersion of the active phase compared to treatment in a neutral or reducing atmosphere reduction [4,16,17], this calcination atmosphere was chosen in order to obtain catalysts that are similar to those usually reported in literature for this type of materials. The three prepared samples were designated Ni-Ce/SBA-15 when the Ce addition

6

preceded the Ni addition, Ce-Ni/SBA-15 when the nickel precursor was added first and co-NiCe/SBA-15 when Ni and Ce were co-impregnated together. Two additional reference catalysts were prepared following the same procedure but with only Ni or Ce addition (samples Ni/SBA-15 and Ce/SBA-15, respectively).

2.2. Catalytic test

The catalytic tests were conducted at atmospheric pressure in a continuous U-shaped fixed-bed flow reactor using 20 mg of catalysts loaded on a quartz wool plug. Prior to the catalytic reaction, each sample was reduced *in situ* at 650°C for about 2 hours in 5 volume% H_2/Ar (30 mL.min^{-1}). After that, the temperature was cooled down to 200°C then increased from about 200°C up to 800°C at a rate of 5°C.min^{-1}. The molar ratio of CH_4 to CO_2 was 1:1 and the gas hourly space velocity (GHSV) was 264 L.g^{-1}.h^{-1}. For stability measurements, the temperature was cooled down to 500°C and maintained at this temperature for 12 hours. The effluent gases were analyzed using a Micro-GC Inficon equipped with a Thermal Conductivity Detector (TCD). The conversions during activity and stability measurements were calculated as follows (*in* and *out* relate to the measurements at the reactor entrance and exit, respectively):

$$CH_4 \text{ Conversion (\%)} = 100*(CH_{4in} - CH_{4out})/CH_{4in}$$

$$CO_2 \text{ Conversion (\%)} = 100*(CO_{2in} - CO_{2out})/CO_{2in}$$

2.3. Characterization techniques

The pore volumes and surface areas were determined from N_2 adsorption-desorption isotherms recorded on an ASAP 2020 (Micromeritics) apparatus. Prior to experiments, the samples were degassed under vacuum for 2 hours at 250°C. XRD patterns were registered on a Brüker D8 diffractometer (Bragg-Brentano, Copper λ= 1.5418 Å). The diffractograms were

recorded both at low angles (2 theta between 0.5° and 5°) and wide angles (2 theta between 5° and 95°) ranges to respectively (i) ascertain the pore structure arrangement of the supports and (ii) evaluate the nature and mean size (calculated using the Scherrer equation) of the supported metal nanoparticles. The morphology and homogeneity of the silica grains were identified by SEM (Scanning Electron Microscopy) on a Hitachi SU-70 SEM-FEG. TEM (Transmission Electron Microscopy) images were registered on a 2010 JEOL JEM-200 electron microscope operating at 200 keV (LaB6 gun) and equipped with an energy dispersive X-ray spectroscopy detector (EDS PGT, spatial resolution below 10 nm) for chemical analyses. TPR experiments were carried out on a Micromeritics Autochem 2910 Instrument equipped with a trap for water removal before TCD detection. The H_2 consumption was followed during heating in 5 volume% H_2/Ar (20 mL.min^{-1}) at a rate of 10°C.min^{-1} from 200°C to 650°C.

3. Results and discussion

3.1. Catalytic activity

The comparison of activity between the different samples is presented first in order to identify if the order of addition of the metals played a role towards catalytic performances of the samples. After reduction of the catalysts at 650°C under 5% H_2/Ar for 2h, the reactor was cooled down to about 200°C and catalytic measurements were carried out while raising again the temperature up to around 750°C. The variations of the conversions of reactants (CH_4 and CO_2) as a function of temperature are shown in Figure 1. Both conversions increased with temperature, reflecting the endothermic character of the dry reforming reaction. However, the CH_4 conversion was always slightly higher than that of CO_2, over the entire temperature range, suggesting some (although limited) decomposition of methane into hydrogen and carbon ($CH_4 \rightarrow 2H_2 + C$) as side reaction [6,18].

In the absence of nickel (Ce/SBA-15 reference catalyst, data not shown), no catalytic activity was observed, thus validating that the active sites for the dry reforming reaction are the metallic nickel nanoparticles. The most active catalyst was Ni-Ce/SBA-15 (Ce impregnated first) on which 100% CH_4 conversion and 90% CO_2 conversion were reached at around 600°C (Fig. 1a,a'). On the contrary, the lowest activity was observed for Ce-Ni/SBA-15 (Ni impregnated first) on which the same conversions as above were attained at 700 (Fig. 1c,c'). The co-impregnation led to better results than Ce-Ni/SBA-15, yet lower than Ni-Ce/SBA-15, but similar to those of the reference catalyst Ni/SBA-15. Therefore, it appears that Ce has to be added previous to Ni in order to ensure a positive effect towards activity, whereas its addition after Ni leads on the contrary to an activity loss. This could be due to a blocking by Ce of some channels where Ni species were previously deposited, thus leading to a hindering of the access to the metal active phase.

All catalysts were relatively stable during 12 hours of catalytic running (data not shown) not only in terms of activity but also with respect to their selectivity. However, the selectivity (reflected in the H_2:CO molar ratio near unity) varied between the different catalysts, as for their activity, in the order Ni-Ce/SBA-15>co-NiCe/SBA-15>Ni/SBA-15>Ce-Ni/SBA-15. Thus, the H_2:CO molar ratio was 0.96 on Ni-Ce/SBA-15 whereas it was only 0.77 on Ce-Ni/SBA-15. Such ratio below 1 suggests the occurrence of side reactions such as RWGS reverse water gas shift reaction [4,6] that therefore occur at higher extent on the Ce-Ni/SBA-15 catalyst than on the Ni-Ce/SBA-15 one. The more limited access to active sites assumed above from conversion data could play a role, enhancing the possibility of side reactions. Therefore, the order of addition of nickel and cerium is important and the best catalyst in terms of both activity and selectivity is obtained when Ni is deposited on the mesoporous support that already contains CeO_2.

(Figure 1)

3.2. Structural properties and morphology

The low angles X-ray diffractograms of the SBA-15 support (uncalcined and calcined) and of the calcined Ni-Ce/SBA-15 and Ce-Ni/SBA-15 samples are shown in Figure 2. After calcination of the fresh SBA-15 silica at 500°C for 9h, the structuring organic agent in the pores was fully eliminated and the silica walls were condensed. This resulted in a decrease in the unit cell parameter from 94.5 Å for the parent uncalcined SBA-15 (Fig. 2 a) to 81.6 Å for the calcined SBA-15 support (Fig. 2b) as calculated from the (100) main diffraction peak. For all samples, the well-resolved peak indexed as (100) and the tiny (110) and (200) peaks are characteristic of the highly ordered p6mm hexagonal mesoporous structure. This structure was preserved after impregnation and calcination treatments (Fig. 2c,d) with however some collapse as indicated by the lower intensity of the peaks.

(Figure 2)

In spite of this collapse attributable to successive impregnation in solution and calcination, high pore volumes and surface areas were still detected after Ni and Ce deposition. All the Ce-Ni/SBA-15, Ni-Ce/SBA-15 and co-NiCe/SBA-15 samples showed a type IV N_2 adsorption-desorption isotherm (Fig. 3) typical of mesoporous materials. The H2-type hysteresis loop observed with a smooth adsorption step and a sharper desorption step revealed non-uniform pore shapes and/or sizes. For all three samples, the BET surface area was in the range 550-650 $m^2.g^{-1}$, and the total pore volume was between 0.3 and 0.4 $cm^3.g^{-1}$. As for the conversion data, the values were the highest for Ni-Ce/SBA-15 in which Ce was impregnated first. Nevertheless, the pore diameter was around 3.4 nm whatever the order of Ni and Ce addition suggesting that, if present, the effect of accessibility inhibition discussed above would rather consist in partial channel blocking than in channel diameter restrictions.

(Figure 3)

The structure and morphology of the samples are further depicted in Figure 4. As seen on the MEB pictures (Fig. 4a,b), the SBA-15 grains of the support were small, almost spherical and homogeneous in size with a length of about 0.3-0.4 µm and diameters in the range 0.4-0.5 µm. This morphology was maintained after catalytic study (spent catalysts). Moreover, TEM images taken both in parallel (Fig. 5a) and perpendicular (Fig. 5b) grain orientations clearly showed the highly ordered linear mesoporous system and hexagonal pore structure characteristic of the SBA-15 structure for all samples.

(Figure 4)

(Figure 5)

3.3. Nanoparticles dispersion and consequences on activity

The darker regions seen on the grey silica grains in the TEM images correspond to metal nanoparticles with higher electronic density than the silica support (Fig. 5). These nanoparticles often appeared regularly aligned along the channels (Fig. 5c) and they were well dispersed inside the pores, even after catalytic tests (Fig. 5d), whatever the sample.

Such preservation of the dispersion upon reaction was also illustrated by EDS measurements. Indeed, in spite of some heterogeneity in the Ni and Ce enrichment between grains, the local compositions were on average not different before and after catalytic tests, with for instance atomic Ni/Si ratios between 0.06 and 0.18 and Ce/Si ratios in the range 0.02 to 0.07 for the co-NiCe/SBA-15 catalyst. This shows the efficiency of the two solvents impregnation method for dispersing rather homogeneously the nanoparticles inside the grains of the SBA-15 support.

Nevertheless, some differences in mean particle sizes were found depending on the order of metal impregnation. This is even better illustrated by the XRD data of calcined samples (Fig.

6 and Table 3). The broad signal observed on all the diffractograms at around 22° is due to the presence of silica with amorphous silica walls. The narrower peaks at $2\Theta = 37°$, 44°, and 63° visible above this signal correspond to nickel oxide nanoparticles (JCPDS 89-5881) with a face-centered cubic lattice (Fm-3m) and a unit cell parameter equal to 8.35 Å. The peaks at $2\Theta = 29°$, 34°, 48°, 57°, and 70° are assignable to cerium oxide (JCPDS 81-0792) with a face-centered cubic lattice and a cell parameter of 5.41 Å. All these peaks are slightly asymmetric indicating that the nanoparticles are not spherical but rather slightly elongated as also seen on TEM images.

(Figure 6)

(Table 3)

The average nanoparticles sizes were calculated by applying the Scherrer equation to the (400) peak for NiO and to the (220) peak for CeO_2 (Table 3), assuming spherical shapes. It thus appeared that NiO and CeO_2 nanoparticles as small as 5-6 nm and 3-4 nm, respectively, were formed over the Ni-Ce/SBA-15 and co-NiCe/SBA-15 catalysts. With respect to NiO, this size is the same as for the Ce-free Ni/SBA-15 sample (NiO nanoparticles with diameter of 6 nm). It is worth noting that the crystalline domains thus calculated for NiO are greater than the diameter of the pores (around 3.5 nm, Table 1). However, this can be explained by the elongated shape of the particles (zoom in Fig. 5b) with diameter around 3-4 nm, smaller than their length (between 4 and 8 nm), forming worm-like aggregates along the channels (Fig. 5c). This also agrees with the slightly asymmetric XRD diffraction peaks for NiO (Fig. 6).

Therefore, contrarily to previous reports (references in Table 1), it is seen that the addition of Ce does not necessarily reduce the nickel particle size. In the present samples, this size was indeed the same in the three following cases: sample with only Ni, sample co-impregnated

with Ni and Ce at the same time, and sample submitted to Ce impregnation first followed by Ni addition. In contrast, the addition of Ni first followed by Ce (Ce-Ni/SBA-15 sample) induced an enlargement of the NiO particle size up to 14 nm (Table 3). At this point, it has to be recalled that the deposited Ni-based nanospecies in this last sample were submitted, during preparation, to a second impregnation step in solution (for Ce deposition) followed by a new calcination step, which may have provoked some instability of the nanoparticles and additional sintering. In fact, this could be the main explanation of the lowest catalytic activity of the Ce-Ni/SBA-15 catalyst, in addition to the accessibility effects discussed above. Indeed, the Ni nanoparticles were on the contrary kept very small on the most active, stable and selective Ni-Ce/SBA-15 catalyst. Therefore, the impregnation of cerium first followed by the addition of nickel is more favorable and this order of impregnation was interestingly also validated in a study on $Ni/La_2O_3/\gamma-Al_2O_3$ catalyst [19] in which lower Ni dispersions and catalytic performances were obtained when impregnating nickel first and then lanthanum.

Interestingly, further information on the spent catalysts was provided by the electron microscopy study. Firstly, the nickel dispersion after stability tests, carried out in reaction conditions for 12 h at 500°C (after heating at 800°C), was found as good as before reaction, as for instance visualized in Figure 5d. Secondly, at this temperature, only very rare carbon nanotubes were observed, attesting of the absence of significant coke formation, in line with the above-mentioned close CH_4 and CO_2 conversions found on all catalysts.

Finally, additional insights on the influence of the order of Ni and Ce addition on the Ni active phase were obtained by TPR (Figure 7 and Table 4). It is known that Ni^{2+} is directly reduced to Ni^0 without passing by intermediate oxides [20]. Two main reduction processes can be distinguished in the ranges 200-400 and 400-650°C. The first peak (200-400°C) is relatively the less intense for the Ce-Ni/SBA-15 sample, while it is the highest for Ni-Ce/SBA-15 catalyst (Table 4). This suggests that easily accessible and more reducible NiO

13

nanoparticles were present on the Ni-Ce/SBA-15 catalyst, in line with porosity data, thus contributing to its highest performances compared to the other samples. On the contrary, the addition of Ce after Ni reduces the accessibility to the NiO nanoparticles as well as their reducibility (Ni Ce-Ni/SBA-15 catalyst).

(Figure 7)

3.4. Comparative catalytic performances

As indicated in the introduction, the preservation of high nickel dispersion combined to an easy access to the active sites appears as a prerequisite to ensure good catalytic performances in dry reforming of methane. In this respect, the smaller Ni-based particles obtained with or without pre-addition of Ce are more active than the larger ones formed when the Ni-containing sample is submitted to new impregnation/calcination for Ce addition.

However, regardless of the order of impregnation, the catalysts tested at medium temperatures in this study showed a better catalytic behavior than the mesoporous catalysts from literature listed in Table 1. The activity performances at 600°C of our catalysts and of Ni/SBA-15 catalysts from bibliography containing or not Ce are compared in Figure 8. At this temperature, more than 80% CH_4 and CO_2 conversions are achieved on our samples while they are around 50% [5] and 60% [6] in bibliographic reports.

A first reason of the good performances of our catalysts lies in the formation of very small NiO nanoparticles; this is not only favored by the mesoporosity of the SBA-15 support, but also strongly ameliorated by the two-solvents method used for metal deposition that helped dispersing and stabilizing the active phase inside the channels, with almost absence of metal deposited outside. Thus, excellent nickel dispersions were obtained, with very small particles sizes below 6 nm, compared to higher sizes reported for comparable materials in literature

(Table 1). The high dispersion in the Ni-Ce/SBA-15 sample is also the result of the enhanced reducibility of the metal species in this sample (Table 4).

(Figure 8)

Besides, thermodynamic features have to be also considered since the dry reforming reaction is known to be thermodynamically limited, thus usually requiring high temperatures to operate in pure reactant mixtures. Nevertheless, thermodynamic data calculated with the HSC chemistry software prove that 90% CH_4 conversion can be achieved at a temperature of 575°C, calculated with respect to the dilution conditions used in our study. Similarly, another study [21] reported an equilibrium temperature of 710°C for 90% CH_4 conversion at the dilution conditions used in their study. Therefore, dilution effects could play a role in this reaction in which the number of formed molecules is doubled in comparison to reactants. Also, we may assume that the SBA-15 silica support can act as a membrane where the diffusion of H_2 outside the pores is higher than that of the remaining products and reactants, shifting the equilibrium to the side of products and increasing the conversions slightly above thermodynamics. Work is in progress to clarify these points.

4. Conclusion

Dry reforming of methane was investigated on Ni and Ce based catalysts supported on SBA-15. Metal sequential impregnations and co-impregnations were employed during the preparation. The characterizations by XRD, SEM and TEM show preserved structure and morphology after impregnation, calcination and catalytic test as well as high dispersion of the active phases inside the porosity due to the "two solvents" impregnation method employed. This method minimized the crystallization of NiO on the external surface of the silica grains.

The most active, stable and selective catalyst was Ni-Ce/SBA-15 sample, prepared by impregnating Ce first then Ni. This was attributed to the smaller particles size obtained on this sample and to its higher reducibility. The activity of the co-NiCe/SBA-15 catalyst was comparable to the Ce-free Ni/SBA-15 catalyst. Contrarily, the impregnation of Ce after Ni causes additional plugging of the pores and formation of larger NiO particles, hindering thus the accessibility of the reactants to the active sites and lowering the activity in dry reforming of methane.

Acknowledgements

Conflicts of Interest

Please note that no conflict of interests affect the corresponding author and the co-authors of this manuscript.

References

[1] V. Havran, M. Dudukovic, C. Lo, Ind. Eng. Chem. Res. 50 (2011) 7089.

[2] D. Pakhare, J. Spivey, RSC Chem. Soc. Rev. 2014. DOI: 10.1039/c3cs60395d.

[3] M.C.J. Bradford, M.A. Vannice, Catal. Rev. Sci. Eng. 41(1) (1999) 1.

[4] J. Zhu, X. Peng, L. Yao, X. Deng, H. Dong, D. Tong, C. Hu, Int. J. Hydrogen Energy 38 (2013) 117.

[5] N. Wang, W. Chu, T. Zhang, X.S. Zhao, Int. J. Hydrogen Energy 37 (2012) 19.

[6] A. Albarazi, P. Beaunier, P. Da Costa, Int. J. Hydrogen Energy 38 (2013) 127.

[7] S. Zhang, S. Muratsugu, N. Ishiguro, M. Tada, ACS Catal. 3 (2013) 1855.

[8] Z. Liu, J. Zhou, K. Cao, W. Yang, H. Gao, Y. Wang, H. Li, Appl. Catal. B 125 (2012) 324.

[9] M. Khavarian, S. Chai, A. Mohamed, Chem. Eng. J. 257 (2014) 200.

[10] W. Donphai, K. Faungnawakij, M. Chareonpanich, J. Limtrakul, Appl. Catal. A 475 (2014) 16.

[11] M.N. Kaydouh, N. El Hassan, A. Davidson, S. Casale, P. Massiani, to be published

[12] D. Zhao, J. Feng, Q. Huo, N. Melosh, G.H. Fredrickson, B.F. Chmelka, G.D. Stucky, Science. 279 (1998) 548.

[13] M. Imperor-Clerc, D. Bazin, M. Appay, P. Beaunier, A. Davidson, Chem. Mater. 16 (2004) 1813.

[14] I. Lopes, N. El Hassan, H. Guerba, G. Wallez, A. Davidson, Chem. Mater. 18 (2006) 5826.

[15] J. Van der Meer, I. Bardez-Giboire, C. Mercier, B. Revel, A. Davidson, R.J. Denoyel, J. Phys. Chem. C 114 (2010) 3507.

[16] J. Sietsma, J. Meeldijk, M. Versluijs-Helder, A. Broersma, A. van Dillen, P. de Jongh, K. de Jong, Chem. Mater. 20 (2008) 2921.

[17] M. Wolters, L. J.W. van Grotel, T. M. Eggenhuisen, J. R.A. Sietsma, K. P. de Jong, P. E. de Jongh, Catalysis Today 163 (2011) 27.

[18] A. Serrano-Lotina, L. Daza, Int. J. Hydrogen Energy 39 (2014) 4089.

[19] R. Yang, C. Xing, C. Lv, L. shi, N. Tsubaki, Appl. Catal. A 385 (2010) 92.

[20] H. Wan, X. Li, S. Ji, B. Huang, K. Wang, C. Li, J. Nat. Gas Chem. 16 (2007) 139.

[21] B. Nagaraja, D. Bulushev, S. Beloshapkin, S. Chansai, J. Ross, Top Catal. 56 (2013) 1686.

List of Figures

List of Tables

Table 4: relative quantification of H_2-TPR peak area (in % of total area) for the different catalysts.

Table 1: Summary of available bibliographic data on DRM using Ni,Ce/mesoporous silica catalysts prepared by wetness impregnation.

Catalysts[a]	Ni content (wt%)	Co-metal	Mean NiO (*Ni^0) particles sizes (nm)	T (°C)	GHSV (L.g^{-1}.h^{-1})	Time on stream (h)	Initial conversions (%)		Final conversions (%)		Ref
							CH$_4$	CO$_2$	CH$_4$	CO$_2$	
Ni/SBA-15	10	5wt% Ce	7.6*	700	36	40	70	70	65	63	5
Ni/Ce-SBA-15	12	Ce/Si=0.04	5.3*				75	76	73	75	
Ni/Ce-SBA-15		Ce/Si=0.06	6.3*				72	76	62	67	
Ni/SBA-15	10	-	12	600	20	24	53	83	39	70	6
Ni/CZ/SBA-15	5	10wt% ceria-zirconia	7				42	39	49	45	
Ni/CZ/SBA-15	10		11				50	66	40	58	
Ni/CZ/SBA-15	15		11				52	43	57	48	
Ni/CZ/SBA-15m.l.	10	10wt% mulit-layered ceria-zirconia	11				48	51	38	43	
Ni/SBA-16		-	9.6*	700	45	100	73	78	52	63	7
NiCe /SBA-16	5	14.6 wt% CeO$_2$	7.5*				72	77	68	74	

Table 2: Textural properties of the calcined Ni and Ce containing samples

Sample	BET surface area $(m^2.g^{-1})$	Total pore volume $(cm^3.g^{-1})$	Pore diameter (nm)
Ce-Ni/SBA-15	650	0.40	3.4
Ni-Ce/SBA-15	607	0.38	3.5
co-NiCe/SBA-15	542	0.32	3.4

Table 3: average sizes (nm) of the NiO and CeO$_2$ nanoparticles in the prepared materials.

Sample name	Composition	Order of impregnation	Ø_{NiO}* (nm)	Ø_{CeO2}* (nm)
Ce/SBA-15	6 wt% Ce	Only Ce	-	5
Ni/SBA-15	5 wt% Ni	Only Ni	5	-
co-NiCe/SBA-15	6 wt% Ce	Co-impregnation	6	3
Ni-Ce/SBA-15		Ce then Ni	6	4
Ce-Ni/SBA-15	5 wt% Ni	Ni then Ce	14	5

*from TEM and XRD measurements (±1 nm)

Table 4: relative quantification of H_2-TPR peak area (in % of total area) for the different catalysts.

Temperature range (°C)	co-NiCe/SBA-15	Ce-Ni/SBA-15	Ni-Ce/SBA-15
200-400	24	34	40
400-650	76	66	60
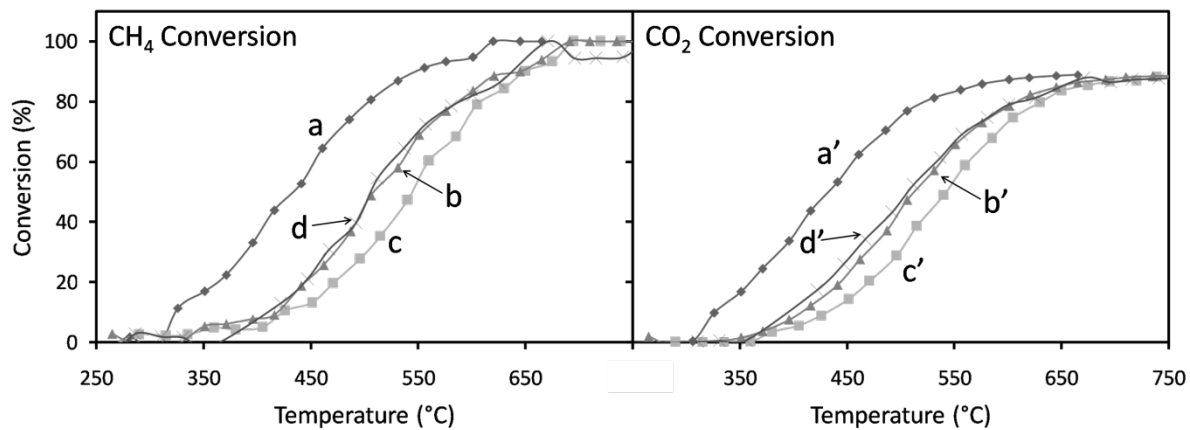
Figure 1: variation of CH_4 (left) and CO_2 (right) conversions as a function of temperature on (a,a') Ni-Ce/SBA-15, (b,b') co-NiCe/SBA-15, (c,c') Ce-Ni/SBA-15 and (d,d') Ni/SBA-15.
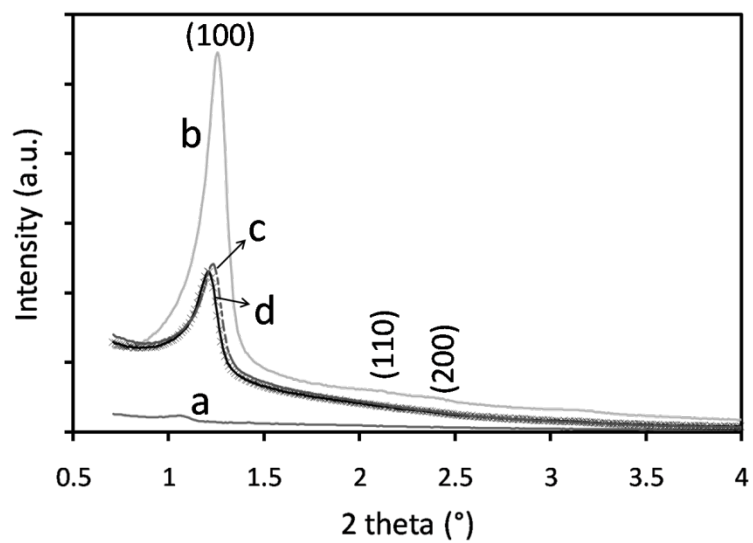
Figure 2: low angles XRD patterns of (a) uncalcined SBA-15, (b) calcined SBA-15, (c) calcined Ni-Ce/SBA-15 and (d) calcined Ce-Ni/SBA-15.
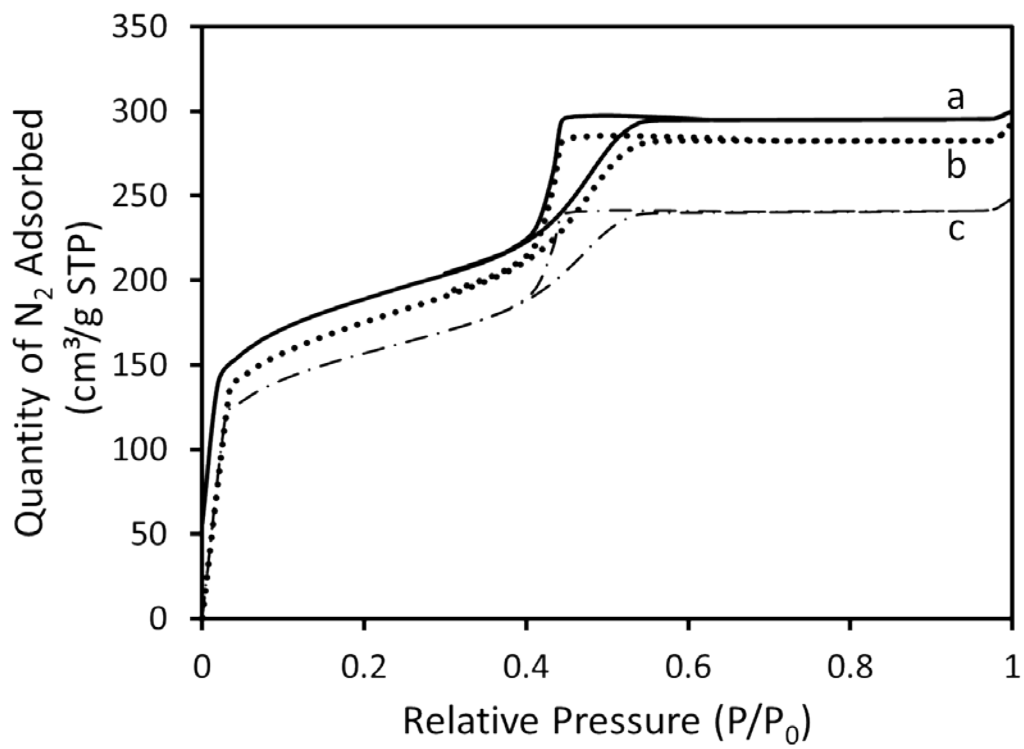
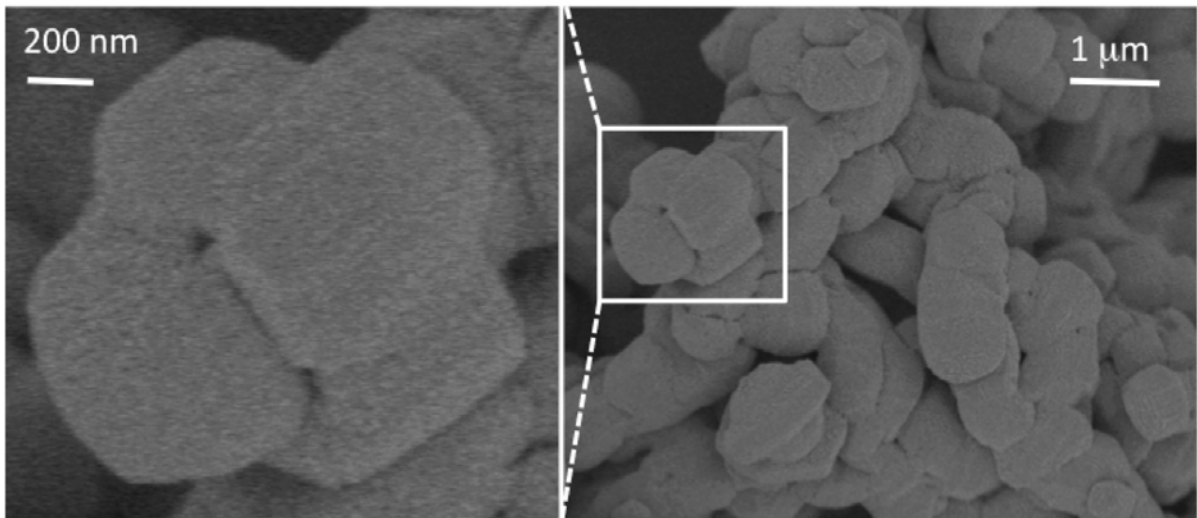**Figure 3:** N$_2$ adsorption-desorption isotherms for samples (a) Ce-Ni/SBA-15, (b) Ni-Ce/SBA-15 and (c) co-NiCe/SBA-15

Figure 4: representative SEM images of the calcined SBA-15 support; on the left, zoom showing the structured surface of the grains..
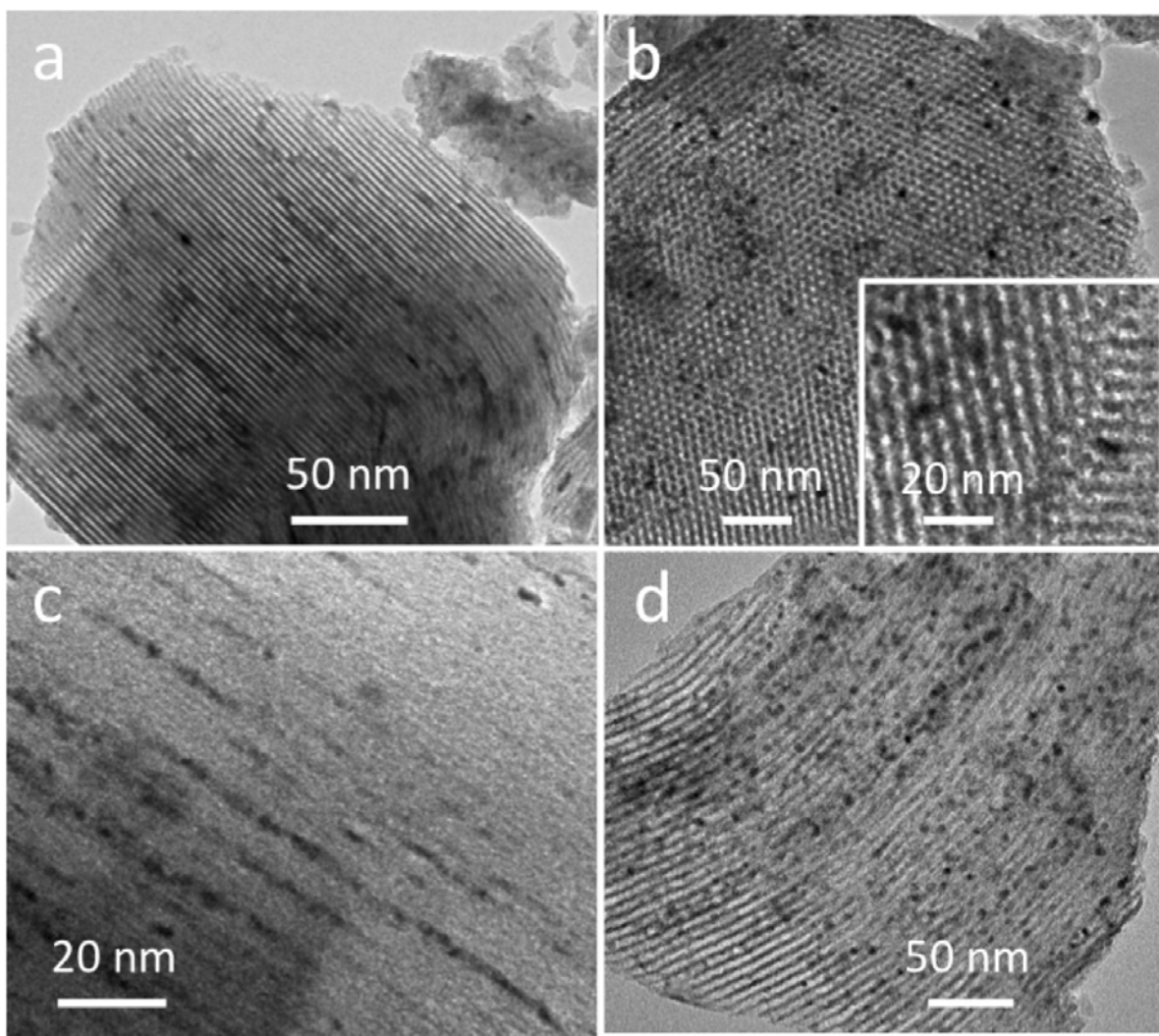
Figure 5: representative TEM micrographs of the (a-c) calcined and (d) spent co-NiCe/SBA-15 catalyst; images taken (a,c,d) parallel or (b) perpendicular to the silica grains.
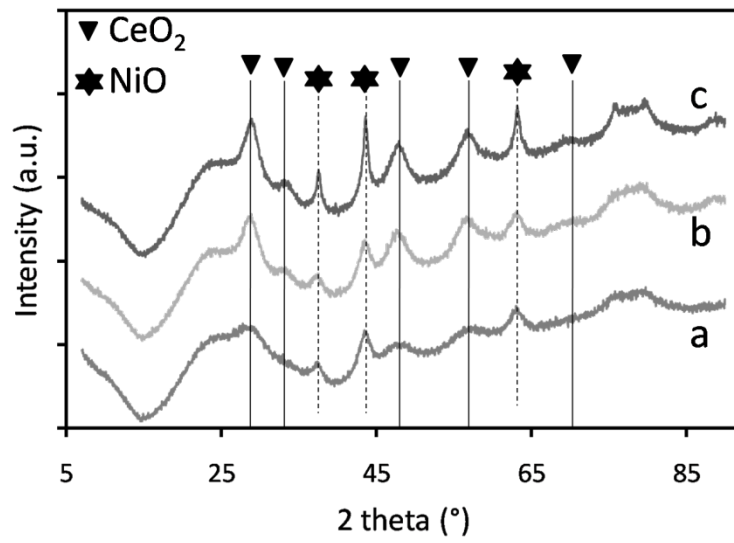
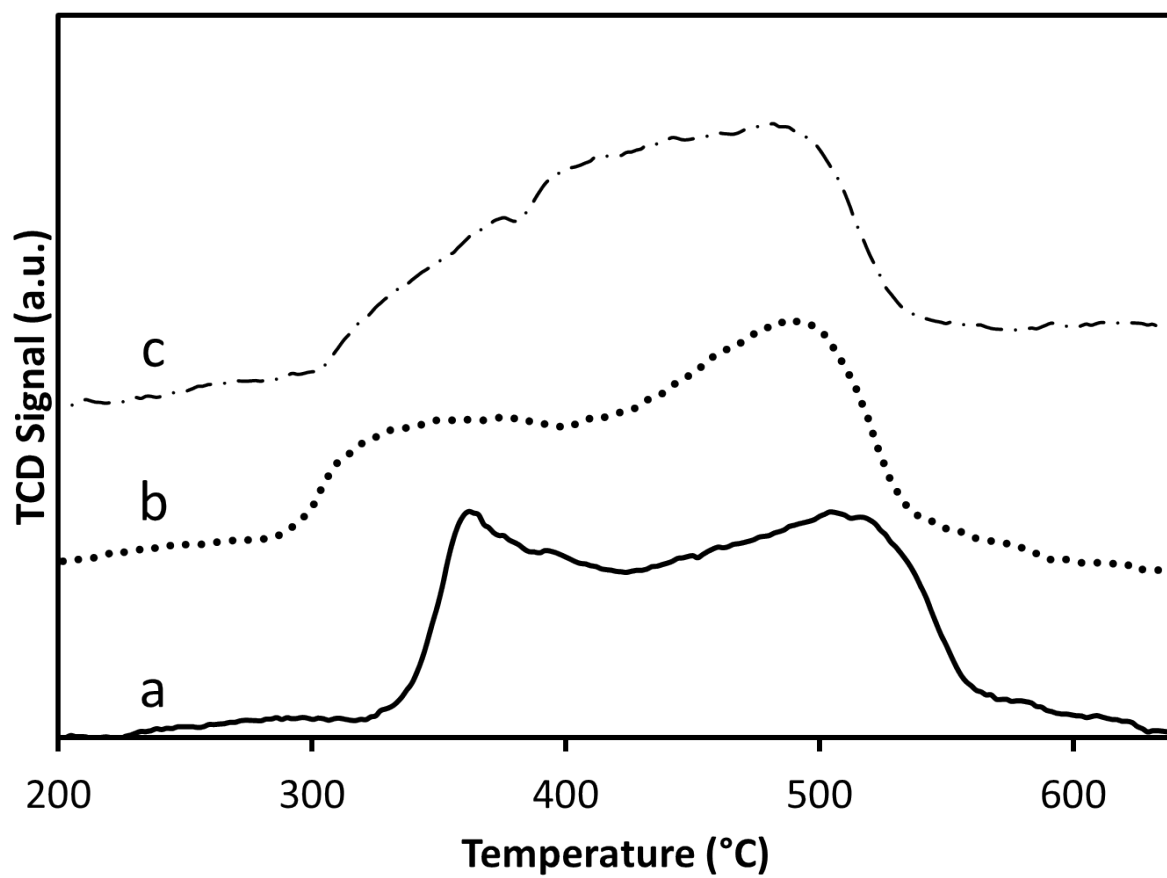**Figure 6:** wide angles XRD patterns of calcined (a) co-NiCe/SBA-15, (b) Ni-Ce/SBA-15 and (c) Ce-Ni/SBA-15.

Figure 7: H$_2$-TPR profiles for (a) Ni-Ce/SBA-15, (b) co-NiCe/SBA-15 and (c) Ce-Ni/SBA-15
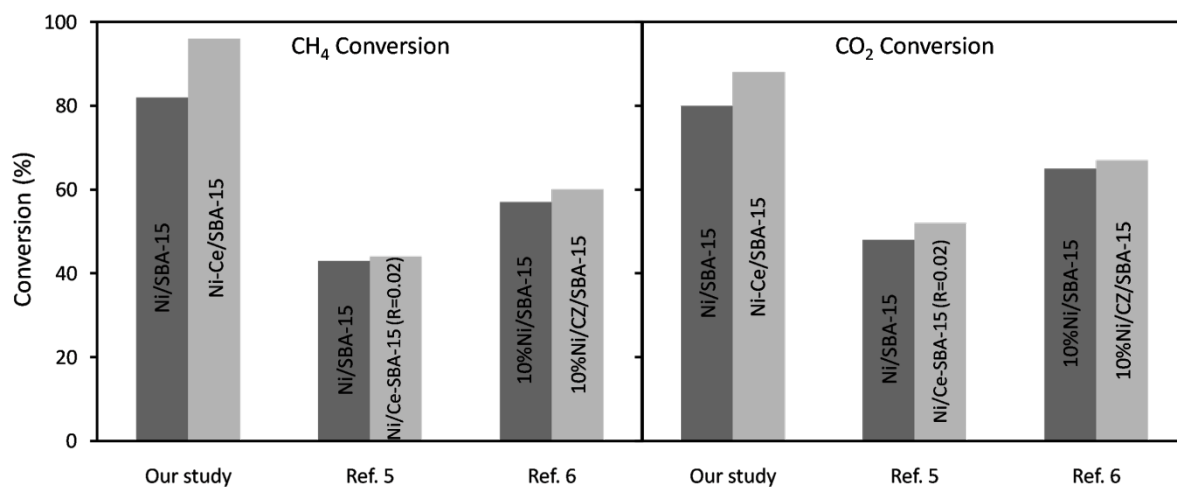
Figure 8: comparisons of CH$_4$ (left) and CO$_2$ (right) conversions obtained at 600°C in this study (GHSV=264 L.g^{-1}.h^{-1}, CO$_2$/CH$_4$=1, 20 mg loading) and in bibliography (Ref. 5: GHSV=36L.g^{-1}.h^{-1},CO$_2$/CH$_4$=1, 100 mg loading; Ref. 6: GHSV=20 L.g^{-1}.h^{-1},CO$_2$/CH$_4$=1, 300 mg loading).